ELSEVIER

International Journal of Heat and Fluid Flow 21 (2000) 562–567

International Journal of HEAT AND FLUID FLOW

www.elsevier.com/locate/ijhff

Effect of particle concentration on fluctuating velocity of the disperse phase for turbulent pipe flow

A.Yu. Varaksin *, Yu.V. Polezhaev, A.F. Polyakov

Department of Heat Transfer, Institute for High Temperatures, Russian Academy of Sciences, Izhorskaya 13/19, Moscow 127412, Russian Federation

Abstract

This paper presents the results of an experimental investigation of the fluctuation velocity distributions of solid particles when they move in the downward gas turbulent pipe flow. The glass particles ($Stk_L \approx 1$) having an average diameter of 50 μm were used as a disperse phase. The average particle mass concentration varied within the range of $\overline{M} = 0$ to 1.2. The results obtained showed the particle fluctuation velocity to be strongly dependent on their mass loading. There has been observed an influence of the particle concentration on the significant increasing of their axial fluctuation velocity in the pipe wall region.

Keywords: Gas–solid flow; Particle velocity fluctuations; Velocity measurements

1. Introduction

Two-phase flows are the most common gas flows seen in nature and industrial applications. Despite many investigations in this field of mechanics, a full understanding of their physics has not been achieved yet, and their parameters still cannot be predicted at a required level of accuracy.

Turbulent air flows containing suspended solid particles were studied by many authors (e.g., Maeda et al., 1980; Lee and Durst, 1982; Tsuji and Morikawa, 1982; Tsuji et al., 1984; Rogers and Eaton, 1990; Kulick et al., 1994; Hosokawa et al., 1998; Varaksin et al., 1998). This paper seeks to study the behavior of solid particles in the downward air turbulent pipe flow. The detailed results of the investigations of time-averaged and fluctuation velocity distributions of solid particles vs. their mass concentration are presented.

2. Experimental setup and procedure

A schematic diagram of our experimental facility designed for studying dilute and dense gas–solid flows is displayed in Fig. 1. The test section is a vertical pipe 1 made of stainless steel and having the internal diameter $D = 46$ mm. The pipe is 2500 mm in length and has 12 mm wide slot 2 in the pipe wall at a distance $L = 1380$ mm from the top end. It is designed for the inlet and outlet of the probing beams of the two-channel triple-beam LDA 10 manufactured by Dantec (Denmark) with whose aid were performed the velocity measurements. To seal the test section hermetically, the slot is covered with transparent windows attached to the pipe by tie pins. The window planes are positioned perpendicularly to the optical axis of transmitting optics 3 of the LDA. The pressurized air produced by compressor 4 is delivered via receiver 5 from tank 6.

To obtain an air flow with solid particles entrained we used feeder 7 operating as follows. Solid particles fed into a bottle (2 l of volume) move to the vertical pipe through pipe 8 of the feeder under the action of the force of gravity. The solid particle mass flux rate varied vs. the size of the feeder outlet aperture.

After passing the receiver and turning section 9 the air flow was mixed with solid particles, and the mixture obtained entered to the test section. After leaving the pipe, the solid particles were utilized by settling tank 10.

The spherical glass particles used in the experiments had the nominal diameter of 50 μm (with the standard deviation 5 μm) and density $\rho_p = 2550$ kg/m^3. The photo of the particles is shown in Fig. 2.

To measure the flow velocity, we used Dantec micron-particle generator 11 (model 55L18) operating on a glycerin–water mixture. The particles generated were 2–3 μm in diameter. The scanning of the pipe cross-section was performed by the Dantec traversing system allowing an automatic movement of the measurement volume along the horizontal axis at an accuracy of 10 μm. The measurement volume had the following characteristics: dimensions – $0.091 \times 0.091 \times 1.32$ mm^3; interference fringe spacing – 3.63 μm; number of fringes – 25.

The velocities of solid particles, single air and two-phase air were measured with the use of the digital output of the Dantec doppler signal processor (model Counter 55L90a). The relative

* Corresponding author. Fax: +7-095-362-5590.

0142-727X/00/$ - see front matter
PII: S0142-727X(00)00045-X

Notation

R	pipe radius
y^+	universal wall coordinate
L	distance from particle entrance to measuring section
d_p	particle diameter
ρ_p	particle density
μ	carrying air dynamic viscosity
ν	carrying air kinematic viscosity
k	carrying air turbulence energy
ε	dissipation rate of the turbulence energy
ℓ	Prandtl mixing length
τ_p	particle dynamic response time, $\equiv \rho_p d_p^2/18\mu C$
C	coefficient for non-Stokesian particles, $\equiv 1 + Re_p^{2/3}/6$
T_f	carrying air characteristic time for the mean motion
T_L	carrying air characteristic time for the large-scale fluctuation motion
U	mean (time-averaged) air velocity
V	mean (time-averaged) particle velocity
$(\overline{u'^2})^{1/2}$	air fluctuation velocity (rms)
$(\overline{v'^2})^{1/2}$	particle fluctuation velocity (rms)
σ_U	air turbulence intensity, $\equiv (\overline{u'^2})^{1/2}/U_{xc}$
σ_V	particle velocity fluctuations intensity, $\equiv (\overline{v'^2})^{1/2}/V_{xc}$
M	particle local mass concentration
$\overline{M}$	mean (across the pipe) particle mass concentration
Φ	particle volume concentration
$\overline{\Phi}$	mean (across the pipe) particle volume concentration
Re_p	particle Reynolds number, $\equiv \lvert U_x - V_x \rvert d_p/\nu$
Re_D	Reynolds number
Stk_f	Stokes number in the mean (time-averaged) motion
Stk_L	Stokes number in the large-scale fluctuation motion

Subscripts

c	parameters at the pipe axis
x	axial direction
r	normal direction
0	initial value

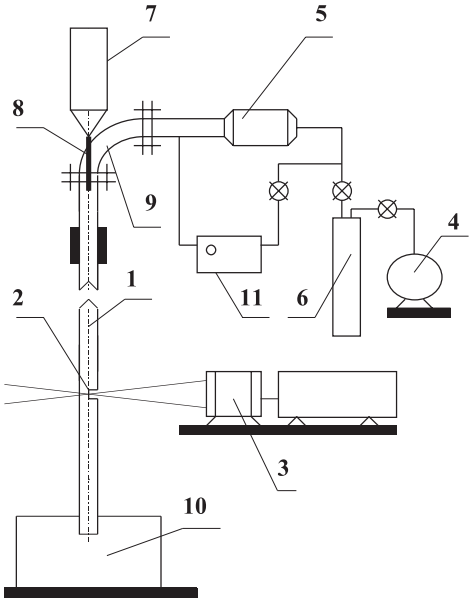

Fig. 1. Experimental setup scheme: (1) vertical pipe; (2) slot for laser beams; (3) optics of the LDA; (4) compressor; (5) receiver; (6) air tank; (7) solid particles feeder; (8) feeder's pipe; (9) turning section; (10) particles settling tank; (11) tracer particles generator.

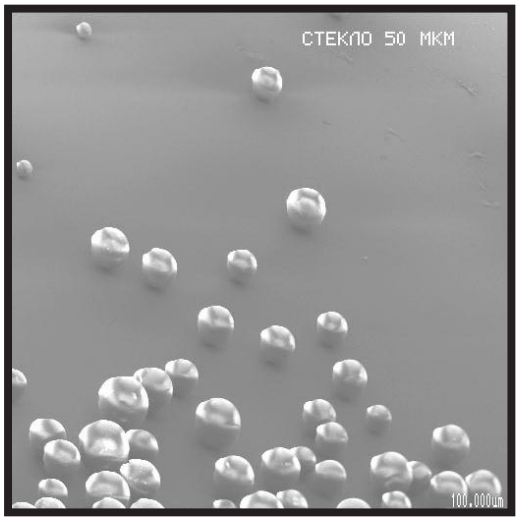

Fig. 2. Photo of 50 μm glass particles used in the experiments.

local mass concentration of the particles was determined against the data sample rate of Doppler signals coming from the disperse phase and the average particle mass loading found by weighing.

Two-phase air velocity measurements were conducted by the use of an amplitude discriminator. Using the discriminator allowed to select the signals from both kinds of particles and to measure air velocity in the presence of the solid particles with suitable accuracy up to $\overline{M} = 0.35$. The method of the two-phase air velocity measurements was described in detail by Varaksin et al. (1996).

The experimental results given below were obtained with the following uncertainties:

2%	for measurements of single air mean velocity;
4%	for measurements of two-phase air mean velocity;
4%	for measurements of particle mean velocity;
7%	for measurements of single air velocity fluctuations;
10%	for measurements of two-phase air velocity fluctuations;
10%	for measurements of particle velocity fluctuations;

The number of samples collected for each data point was about 4000 for correct statistical treatment of the measured parameters.

3. Results and discussion

All the measurements described here were performed at the mean (time-averaged) air flow velocity on the pipe axis

$U_{xc} = 5.2$ m/s. The Reynolds number based on the pipe diameter was $Re_D = 15{,}300$. The distance from the particle entrance section to the measuring cross-section was equal, $L = 1380$ mm ($L/D = 30$).

The experimental results obtained for the particle mass concentration distributions, mean and fluctuation velocity distributions for particles, single air and two-phase air are given below.

Fig. 3 shows three used values of the particle mass concentration and corresponding volume concentrations. It also demonstrates the scheme of the inter-phase interactions, taken from the work by Elghobashi (1991). The following conclusions can be made:

1. the low value of the particle concentration used in the experiments practically corresponds to the dilute suspension flow without any back influence of the particles on the carrier phase characteristics;
2. the middle particle concentration exists in the central region of the dilute suspension flow with the particle influence on the carrier phase parameters;
3. the high value of the particle concentration corresponds to the concentration boundary between the dilute and dense suspension flows, i.e. to the flow where there are interactions between the particles.

Thus, in our experiments we made an attempt to describe all possible types of the heterogeneous flows relative to the disperse phase concentration.

Fig. 4 shows the distributions of the particle local mass concentration vs. their average (over the pipe cross-section) mass loading ($r/R = 0$ refers to the pipe axis). It can be seen that the distributions of the particles are almost uniform with an exception of the case when $\overline{M} = 1.2$. For this mass loading, the particle local concentration becomes higher (as compared with the average particle loading) in the region near the pipe axis and drops near the pipe wall. This phenomenon is, apparently, caused by the pipe being length insufficient to create an approximately uniform distribution of the particles by the turbulent flow.

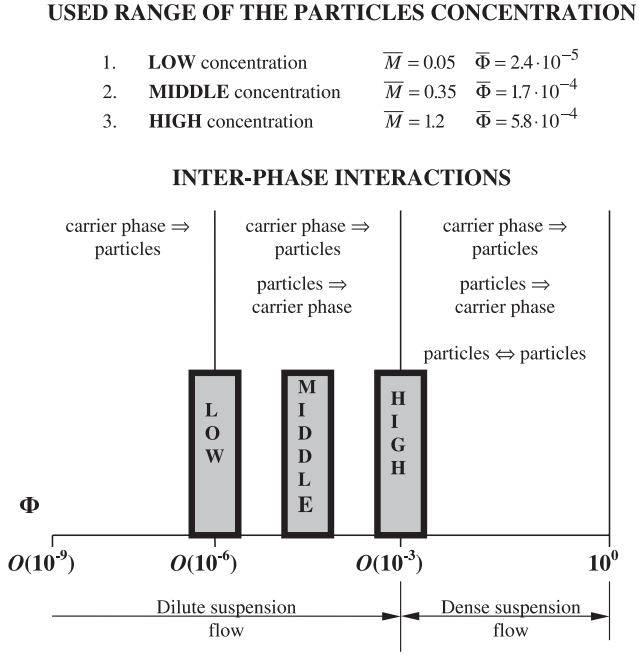

Fig. 3. Range of particle concentration and corresponding phase interactions.

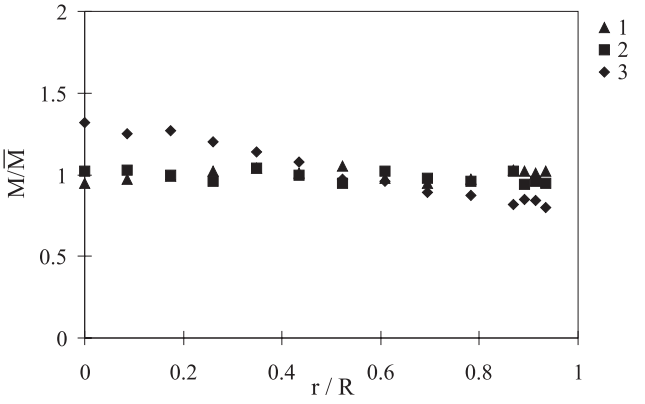

Fig. 4. Mass concentration distributions for 50 μm glass particles: (1) $\overline{M} = 0.05$; (2) $\overline{M} = 0.35$; (3) $\overline{M} = 1.2$.

Fig. 5 demonstrates the profiles of the mean (time-averaged) velocities for single air and solid particles. The two-phase air mean velocity distributions (they are not shown in the figure) were identical to that for single air up to $\overline{M} = 0.35$. Some differences between these profiles lie within the limits of experimental uncertainty. This figure shows the axial mean velocity of the particles to be greater than that of the carrying air within the whole cross-section of the pipe. This circumstance confirms the glass particle acceleration to turn to zero in the measurement cross-section. The completeness of the particle acceleration may be characterized by their Stokes number for the mean (time-averaged) motion

$$Stk_f = \tau_p / T_f, \tag{1}$$

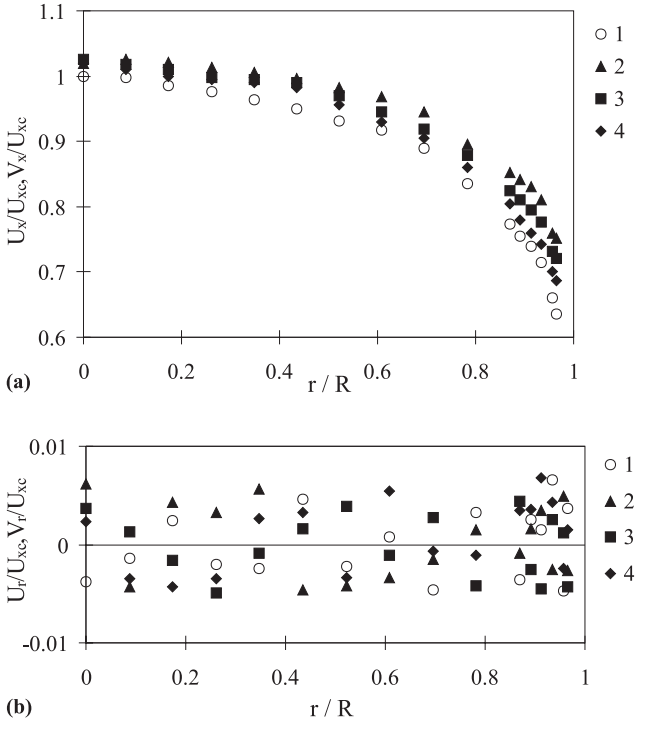

Fig. 5. The distributions of (a) axial and (b) normal mean velocities for air and 50 μm glass particles: (1) air ($\overline{M} = 0$); (2) particles ($\overline{M} = 0.05$); (3) particles ($\overline{M} = 0.35$); (4) particles ($\overline{M} = 1.2$).

where the response time of particles is defined as

$$\tau_p = \frac{\rho_p d_p^2}{18\mu(1 + Re_p^{2/3}/6)} \quad (2)$$

and the characteristic time of the carrier phase for the time-averaged motion may be written as

$$T_f = L/U_{xc}. \quad (3)$$

For the used 50 μm glass particles under the conditions of the present investigation we can obtain easily from (1)–(3) that $Stk_f = 0.07$ (at the pipe axis).

Fig. 5(a) shows the particle axial mean velocity distribution to have a smoother shape as compared with that for air (for the region where $0 < r/R < 0.9$). The velocity of the particles in the near-wall region decreases and strongly depends upon their mass loading. Therefore, the larger value of the particle concentration leads to the more abrupt shape of their axial mean velocity distribution. The increasing of the concentration is likely to result in an intensive exchanging of momentum between the phases in the time-averaged motion. This, in its turn, makes the shapes of velocity profiles of particles and carrying air close to each other. Another probable reason of the particle velocity decrease at high mass loading ($\overline{M} = 1.2$) is momentum lost due to the particle–particle and particle–wall interactions.

Fig. 5(b) shows the mean velocity distributions for single air and for particles in the normal direction to the pipe wall. These distributions evidently demonstrate the value of these characteristics for both the phases of the heterogeneous flow to be very close to zero (deviations from zero lie within the limits of experimental errors).

In Fig. 6 are given the distributions of the axial mean velocity for air and particles in the universal coordinates

$$U^+ = f(y^+), \quad V^+ = f(y^+), \quad (4)$$

where $U^+ = U_x/U_*$; $V^+ = V_x/U_*$; $y^+ = (R - r)U_*/v$; U_* is the shear velocity. The value of the shear velocity is calculated by the following expression:

$$U_* = U_m(\xi/8)^{1/2}. \quad (5)$$

Here $U_m = 2/R^2 \int_0^R U_x(r) r\, dr$ is the air velocity averaged over the pipe cross-section and ξ is the friction coefficient found by the Blasius formula $\xi = 0.316/Re_D^{0.25}$.

In Fig. 6 are shown the curves $U^+ = y^+$ corresponding to the viscous sublayer and $U^+ = 2.5\ln y^+ + 5.5$, which is a universal function describing the distribution of averaged velocities of stabilized turbulent flows in channel and pipes. The comparison of these dependences with the experimental data obtained shows the latter to describe both the area obeying the "logarithmic wall law" ($y^+ > 30$) and the buffer region near the wall. At $y^+ < 80$, the experimental data obey the semi-logarithmic dependence. However, inside the flow core the experimental points are not on this curve. This may be explained by insufficient development of the profile of velocities caused, in its turn, by the low length $L/D = 30$ and, apparently, by the influence of the initial turbulence.

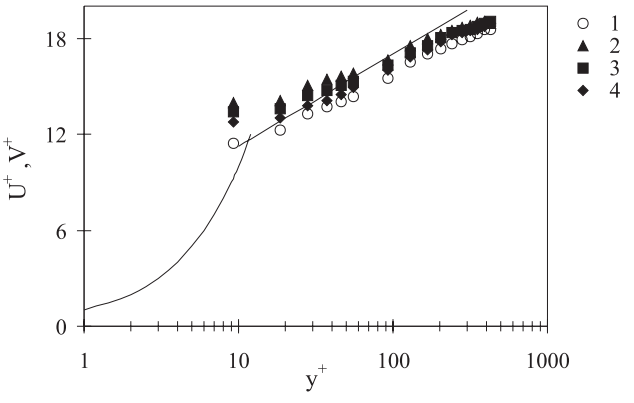

Fig. 6. Mean velocity distributions for air and 50 μm glass particles in wall coordinates: (1) air ($\overline{M} = 0$); (2) particles ($\overline{M} = 0.05$); (3) particles ($\overline{M} = 0.35$); (4) particles ($\overline{M} = 1.2$).

The experimental results obtained and related to the distributions of the particle fluctuation velocities are discussed below. Let us turn to the analysis of possible reasons of velocity fluctuations of solid particles moving in the turbulent flow (see Fig. 7):

1. appearance of the particle velocity turbulent fluctuations due to their involvement in the fluctuating motion by turbulent eddies of the carrying air;
2. appearance of the particle velocity fluctuations caused by the use of the polydisperse particles in the experiments, i.e. particles having different sizes (the difference in time-averaged velocities of such particles causes the interpretation of their values obtained experimentally as certain fluctuation velocities);
3. the variations of particle velocities caused by interactions between themselves and the wall;
4. appearance of the particle velocity fluctuations due to particle migration in the region with shear of time-averaged particle velocity.

Note that the particle velocity fluctuations observed are likely to be directly concerned with the error of particle velocity measurements which is greater than that of the single air flow.

Some of the reasons described above for the particle velocity fluctuations have been studied previously. So, the

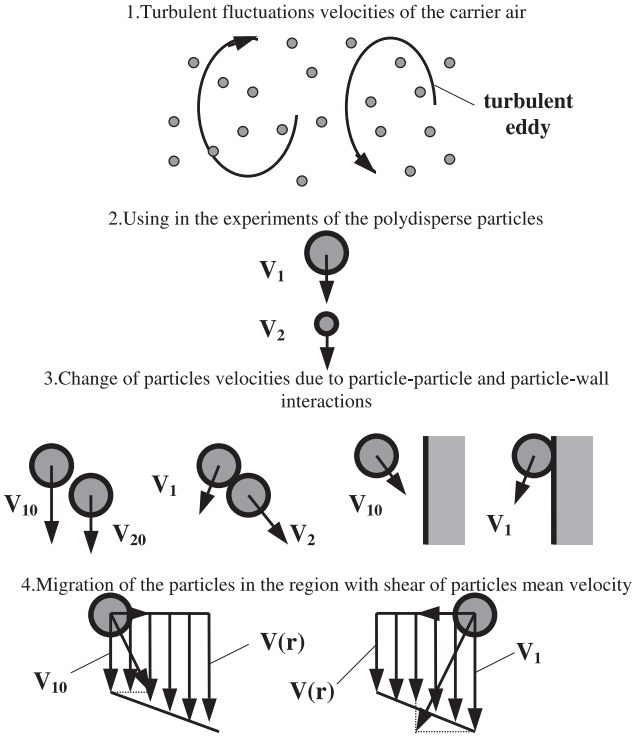

Fig. 7. Main reasons of the appearance of particle velocity fluctuations in a turbulent flow.

change of the particle velocity due to particle–particle collisions was studied by Sommerfeld (1991, 1995). Qualitative estimations of the effect of the carrying phase averaged velocity gradient upon the intensity of particle velocity fluctuations were given by Liljegren (1993, 1994). The reasons for the particle velocity fluctuation appearance and particle–wall interaction were considered in detail by Sommerfeld et al. (1990, 1992, 1993).

Fig. 8 demonstrates the distributions of the intensity of axial velocity fluctuations for the single air, two-phase air and for glass particles. It can be seen from this figure to be ca. $\sigma_{V_x} \approx 8\%$ near the pipe axis at low mass loading ($\overline{M} = 0.05$). This value exceeds the corresponding one for the air equal to $\sigma_{U_x} \approx 5.5\%$ ($\overline{M} = 0.05$). The particle velocity fluctuation intensities drop with growing mass loading. So, at mass loadings $\overline{M} = 0.35$ and $\overline{M} = 1.2$, they are $\sigma_{V_x} \approx 7\%$ and $\sigma_{V_x} \approx 5\%$, respectively. The particle velocity fluctuations observed in the para-axial region are mainly caused, on the one hand, by the particle entrainment by carrying air turbulent eddies and, on the other hand, by particle velocity fluctuations induced by their polydispersity. The particle Stokes number written in the following form characterizes the inertia of the particles in the large-scale turbulent motion:

$$Stk_L = \tau_p / T_L, \tag{6}$$

where the integral time scale of the turbulence (life-time of the large-scale turbulent eddies) T_L may be represented as

$$T_L = c_\mu^{1/2} k/\varepsilon = \ell / c_\mu^{1/4} k^{1/2} \quad (c_\mu = 0.09). \tag{7}$$

The turbulence energy of the carrier phase k may be estimated with the use of the following expression:

$$2k = \sum_i \overline{u_i'^2} \approx \overline{u_x'^2} + \overline{u_r'^2} + (\overline{u_x'^2} + \overline{u_r'^2})/2. \tag{8}$$

For 50 μm glass particles at our experimental conditions, we obtain with the use of (6)–(8) the Stokes number to be approximately equal to unity ($Stk_L \approx 1$ at the pipe axis). Then we conclude the particles used to be relatively easily involved in the large-scale turbulent motion. Therefore, they take up the energy from carrying air turbulent vortices. This effect increases with growing particle mass concentration. The damping of air turbulence intensity causes decreasing of the particle velocity turbulent fluctuations observed in our experiments.

The particle–particle collisions begin to play a significant role in the formation of statistical characteristics of the disperse phase at high mass concentration ($\overline{M} = 1.2$). Intensive exchange of momentum between the particles leads to the proximity of their velocities. Thus, the particle–particle collisions are an additional factor explaining decreasing of their velocity fluctuations induced by the difference of their sizes.

Fig. 8 shows the particle velocity fluctuations intensity to increase with the approach to the pipe wall. So, the intensity of the particle velocity fluctuation near the distance 2 mm from the pipe wall is ca. $\sigma_{V_x} \approx 12\%$ at low particle mass loading ($\overline{M} = 0.05$). This value exceeds that for carrying air equal to $\sigma_{U_x} \approx 10\%$ at the same point of measurement. The intensity of the particle velocity fluctuations increases with growing mass concentration. So, the particle fluctuation intensities in the near-wall region are $\sigma_{V_x} \approx 16\%$ and $\sigma_{V_x} \approx 24\%$ at mass concentrations $\overline{M} = 0.35$ and 1.2, respectively. It should be emphasized that the inertia of the particles (their Stokes number Stk_L) strongly increases in the region near the pipe wall, because the characteristic time T_L of carrying energy turbulent eddies becomes much less than that at the pipe axis. Therefore, the rate of particles involving in the fluctuation motion and the damping of the air turbulence intensity near the pipe wall are much smaller compared with the pipe axis region (this may be seen from Fig. 8). In this instance, the explanation of the high values of particle velocity fluctuations near the pipe wall observed in the experiments is quite difficult. The existence of large shear of the carrying air time-averaged velocity is likely to be the main consideration of the particle fluctuations growing in this pipe region ($0.6 < r/R < 0.9$). The shear of the air velocity results in the formation of the particle velocity gradient increasing with the particle concentration (see Fig. 5(a)). The particle migration in the region with shear of their time-averaged velocities is what may cause high values of the particle fluctuations observed.

Fig. 9 shows the distributions of the velocity fluctuations intensity in the direction normal to the wall for single air, two-phase air and glass particles. We can see from this figure the particle velocity fluctuations intensity to be less than one for single air over the whole pipe cross-section. Involving of the particles into the turbulent motion is certain to be the main cause of the particle velocity fluctuations observed in the normal direction. The difference of particle sizes does not affect the appearance of their fluctuations in this direction, unlike the case of fluctuations in the axial directions described above.

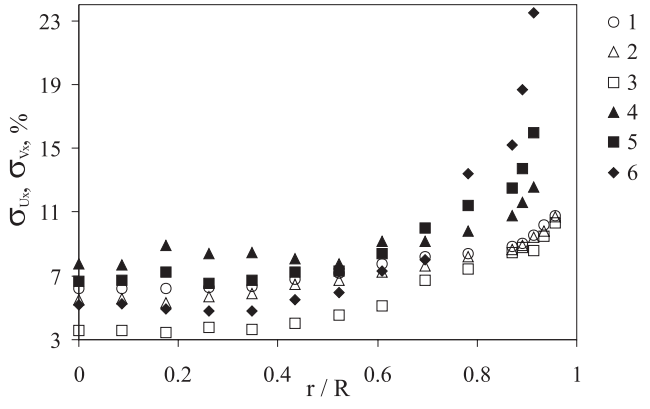

Fig. 8. Distributions of the intensity of fluctuations in the axial direction for air and 50 μm glass particles: (1) air ($\overline{M} = 0$); (2) air ($\overline{M} = 0.05$); (3) air ($\overline{M} = 0.35$); (4) particles ($\overline{M} = 0.05$); (5) particles ($\overline{M} = 0.35$); (6) particles ($\overline{M} = 1.2$).

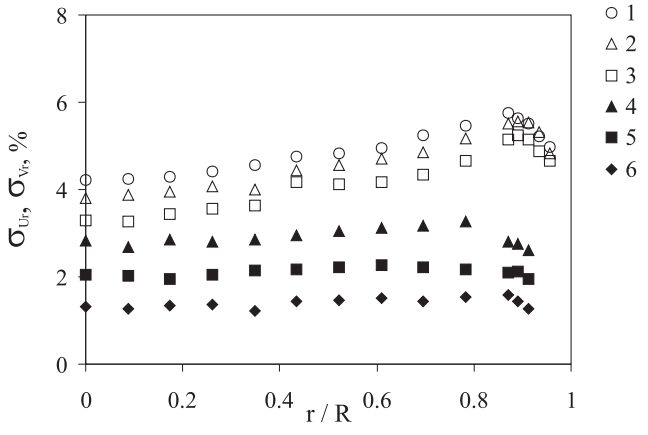

Fig. 9. Distributions of the intensity of fluctuations in the direction normal to the wall for air and 50 μm glass particles: (1) air ($\overline{M} = 0$); (2) air ($\overline{M} = 0.05$); (3) air ($\overline{M} = 0.35$); (4) particles ($\overline{M} = 0.05$); (5) particles ($\overline{M} = 0.35$); (6) particles ($\overline{M} = 1.2$).

This is due to the proximity to zero of the transversal component of the time-averaged velocity taking place for particles having various diameters (see Fig. 5(b)). The growing of the particle concentration leads to an intensification of the exchange of momentum between the phases in the fluctuation motion, which in turn, results in reduction of the air turbulence intensity in the normal direction. The particle velocity fluctuations decrease due to this damping of the carrier phase turbulent fluctuations. The neighborhood of pipe wall limits the particle motion in the normal direction. Hence, the closer they are to the wall, the lower the particle velocity fluctuations are, turning to zero on the wall.

4. Concluding remarks

The behavior of the particles in downward turbulent air–solid pipe flow has been experimentally studied. The distributions of the particle mean velocity and particle velocity fluctuations in the flow direction and that normal to the pipe wall have been measured. The ratio of the particle response time to the large-scale turbulence time scale was about 1 (at the pipe axis). The experiments were performed within a wide range of particle concentrations. The increasing of the particle concentration was obviously observed to result in the damping of their axial velocity fluctuations in the para-axial and, on the contrary, to the significant growing of these values near the pipe wall.

The main reasons for the solid particle velocity fluctuations have been described.

Acknowledgements

The authors were partly supported by the Russian Foundation for Basic Research (projects nos. 98-02-17323 and 00-02-17713) and the President Grant (no. 00-15-99016) for leading scientific schools (Yu.V. Polezhaev).

References

Elghobashi, S., 1991. Particle-laden turbulent flows: direct simulation and closure models. Appl. Sci. Res. 48, 301–314.

Hosokawa, S., Tomiyama, M., Morimura, M., Fujiwara, S., Sakaguchi, T., 1998. Influences of relative velocity on turbulent intensity in gas–solid two-phase flow in a vertical pipe. In: Proceedings of the Third International Conference on Multiphase Flow, Lyon, France, Paper 279 (CD-ROM).

Kulick, J.D., Fessler, J.R., Eaton, J.K., 1994. Particle response and turbulence modification in fully developed channel flow. J. Fluid Mech. 277, 109–134.

Lee, S.L., Durst, F., 1982. On the motion of particles in turbulent duct flows. Int. J. Multiphase Flow 8 (2), 125–146.

Liljegren, L.M., 1993. The effect of a mean fluid velocity gradient on the streamwise velocity variance of a particle suspended in a turbulent flow. Int. J. Multiphase Flow 19 (3), 471–484.

Liljegren, L.M., 1994. The influence of a mean fluid velocity gradient on the particle-fluid velocity covariance. Int. J. Multiphase Flow 20 (5), 969–977.

Maeda, M., Hishida, K., Furutani, T., 1980. Velocity distributions of air-solid suspension in upward pipe flow (effect of particles on air velocity distributions). Trans. Jpn. Soc. Mech. Eng. Ser. B 46, 2313–2320.

Rogers, C.B., Eaton, J.K., 1990. The behavior of solid particles in a vertical turbulent boundary layer in air. Int. J. Multiphase Flow 16 (5), 819–834.

Sommerfeld, M., 1990. Numerical simulation of the particle dispersion in turbulent flows including particle lift forces and different particle/wall collision models. Numerical methods for multiphase flows. ASME FED 91, 11–18. ASME, New York.

Sommerfeld, M., 1991. On the particle velocity fluctuations in turbulent particulate two-phase flows. Turbulence modification in multiphase flows. ASME FED 110, 15–21. ASME, New York.

Sommerfeld, M., 1992. Modelling of particle–wall collisions in confined gas-particle flows. Int. J. Multiphase Flow 18 (6), 905–926.

Sommerfeld, M., 1995. The importance of inter-particle collisions in horizontal gas–solid channel flow. Gas-particle flows. ASME FED 228, 335–345. ASME, New York.

Sommerfeld, M., Huber, N., Wachter, P., 1993. Particle–wall collisions: experimental studies and numerical models. Gas–solid flows. ASME FED 166, 183–191. ASME, New York.

Tsuji, Y., Morikawa, Y., 1982. LDV Measurements of an air-solid two-phase flow in a horizontal pipe. J. Fluid Mech. 120, 385–409.

Tsuji, Y., Morikawa, Y., Shiomi, H., 1984. LDV measurements of an air-solid two-phase flow in a vertical pipe. J. Fluid Mech. 139, 417–434.

Varaksin, A.Yu., Kurosaki, Y., Satoh, I., Polezhaev, Yu.V., Polyakov, A.F., 1998. Experimental study of the direct influence of the small particles on the carrier air turbulence intensity for pipe flow. In: Proceedings of the Third International Conference on Multiphase Flow, Lyon, France, Paper 368 (CD-ROM).

Varaksin, A.Yu., Polezhaev, Yu.V., Polyakov, A.F., 1996. Efficiency of amplitude selection of signals in a study of heterogeneous flows using a laser-Doppler anemometer. Meas. Tech. 39 (6), 645–651.